

Research Article

# Study of Hopcalite ( $\text{CuMnO}_x$ ) Catalysts Prepared Through A Novel Route for the Oxidation of Carbon Monoxide at Low Temperature

Subhashish Dey<sup>1\*</sup>, Ganesh Chandra Dhal<sup>1</sup>, Devendra Mohan<sup>1</sup>, Ram Prasad<sup>2</sup>

<sup>1</sup>Department of Civil Engineering, IIT (BHU), Varanasi, India

<sup>2</sup>Department of Chemical Engineering and Technology, IIT (BHU), Varanasi, India

Received: 28<sup>th</sup> December 2016; Revised: 19<sup>th</sup> April 2017; Accepted: 19<sup>th</sup> April 2017;  
Available online: 27<sup>th</sup> October 2017; Published regularly: December 2017

## Abstract

Carbon monoxide (CO) is a poisonous gas, recognized as a silent killer. The gas is produced by incomplete combustion of carbonaceous fuel. Recent studies have shown that hopcalite group is one of the promising catalysts for CO oxidation at low temperature. In this study, hopcalite ( $\text{CuMnO}_x$ ) catalysts were prepared by  $\text{KMnO}_4$  co-precipitation method followed by washing, drying the precipitate at different temperatures (22, 50, 90, 110, and 120 °C) for 12 h in an oven and subsequent calcination at 300 °C in stagnant air, flowing air and in a reactive gas mixture of (4.5% CO in air) to do the reactive calcination (RC). The prepared catalysts were characterized by XRD, FTIR, SEM-EDX, XPS, and BET techniques. The activity of the catalysts was evaluated in a tubular reactor under the following conditions: 100 mg catalyst, 2.5% CO in air, total flow rate 60 mL/min and temperature varying from ambient to a higher value, at which complete oxidation of CO was achieved. The order of calcination strategies based on activity for hopcalite catalysts was observed to be as: RC > flowing air > stagnant air. In the kinetics study of  $\text{CuMnO}_x$  catalyst prepared in RC conditions the frequency factor and activation energy were found to be  $5.856 \times 10^5$  (g.mol)/(g<sub>cat</sub>.h) and 36.98 kJ/gmol, respectively. Copyright © 2017 BCREC Group. All rights reserved

**Keywords:** Carbon monoxide; Catalytic oxidation;  $\text{CuMnO}_x$ ; Hopcalite catalysts; Co-precipitation; Reactive Calcination

**How to Cite:** Dey, S., Dhal, G.C., Mohan, D., Prasad, R. (2017). Study of Hopcalite ( $\text{CuMnO}_x$ ) Catalysts Prepared through A Novel Route for the Oxidation of Carbon Monoxide at Low Temperature. *Bulletin of Chemical Reaction Engineering & Catalysis*, 12 (3): 393-407 (doi:10.9767/bcrec.12.3.882.393-407)

**Permalink/DOI:** <https://doi.org/10.9767/bcrec.12.3.882.393-407>

## 1. Introduction

The enormous interest has arisen for the oxidation of carbon monoxide (CO) at the ambient conditions, due to its emissions from various sources and a number of adverse effects on public health and an environment. Thus, CO has

been termed as the silent killer for the 21<sup>st</sup> century [1]. CO also called carbonous oxide is a colorless, odorless, tasteless, and nonirritating gas, which makes it difficult for humans to detect and is slightly lighter than air [12]. The toxicity of CO is due to its affinity for hemoglobin in the blood stream. Carbon monoxide is a poisonous and life-threatening gas to humans and other forms of air-breathing life, as inhaling even relatively small concentration of it can lead to

\* Corresponding Author.

E-mail: subhasdey633@gmail.com (Dey, S.)

serious injury, neurological damage and possibly death. When CO enters the bloodstream it combines with hemoglobin and forms carboxy-hemoglobin, which reduces the oxygen-carrying ability of the blood. The huge amounts of carbon monoxide are emitted in the world, mainly from transportation; fireplaces; industrial and domestic activities [15]. The oxidation of CO at low-temperature is gaining a huge attention at a current scenario due to the application in many different fields. These include fire-fighting and mining [2] in the form of breathing apparatus. The three-fourth of all the hydrocarbons and CO are emitted during, a test run of the car in Cold-start conditions [3].

In the beginning, more interest has been focused on catalytic control of CO emissions from automobile exhaust because it is dangerous for the environment [22]. On start-up car exhaust catalysts take a little time to become effective, and this primarily due to the time required to heat the catalyst using the exothermicity of the combustion reactions [21]. If the catalyst could be added that was very efficient for combustion at lower temperatures, then this initial warm-up period could be shortened and the cold start problem can be solved [23]. In the past 35 years, catalytic converters have been installed on more than 1000 million vehicles around the world. The choice of the appropriate catalyst is an important step for improving the environment [14].

After research for decades, two main types of catalysts for CO oxidation near room temperatures have been developed, the first type includes high surface area precious metal based catalysts and the second one incorporates transition metal oxide-based catalysts [13]. The most effective catalyst for CO oxidation at a low temperature in many years is known as hopcalite catalyst ( $\text{CuMnO}_x$ ), which is a mixture of copper manganese oxide [4,7]. Sometimes it also contains  $\text{Co}_2\text{O}_3$  and  $\text{Ag}_2\text{O}$ . The activity of copper, manganese oxide mixture for low-temperature oxidation of CO is discovered by Lamb in the year 1920 [8].

The catalytic properties of such a system called hopcalite were confirmed by Jones and Taylor in the year 1923; since that instant, hopcalite has become a well-known oxidation catalyst at a low temperature. Literature survey concludes that hopcalite catalyst is highly active in the amorphous state even at room temperature [9]. It is observed that hopcalite lose their activity after exposition at temperatures above 500 °C, where crystallization of the spinel  $\text{CuMn}_2\text{O}_4$  occurs [4-6]. However, Schwab

and Kanungo [5] reported that crystalline  $\text{Cu}_2\text{MnO}_4$  is also active. These catalysts have been employed to oxidize environmentally damaging gasses at ambient temperature. A lot of interest has been applied to the modification of hopcalite catalyst in order to eliminate its faults of moisture deactivation and low activity [17]. The preparation of the catalyst by other methods including anti-solvent precipitation method, sol-gel method [7,11] was reported to give better conversion than commercial hopcalite. The structural, morphological, and activation property of  $\text{CuMnO}_x$  catalyst is depending on the preparation methods. Therefore, in the present study,  $\text{CuMnO}_x$  catalysts were prepared using a novel redox method and their performance for CO oxidation was evaluated near ambient conditions [10,19].

In the present study,  $\text{CuMnO}_x$  catalysts are prepared by co-precipitation method, and their performance for CO oxidation is evaluated at a low temperature [11,19]. The effect of preparation parameters, drying time and calcination condition is highly affected by the performance of  $\text{CuMnO}_x$  catalyst for CO oxidation [16]. The precursor material to the active  $\text{CuMnO}_x$  for CO oxidation catalyst is a well-mixed copper nitrate and manganese acetate. This is subsequently heat treated using a relatively standard calcination procedure in air to form the active catalyst [15,20]. The  $\text{CuMnO}_x$  catalyst being produced under oxygen-rich atmosphere conditions and its confirmation of the retardation of copper oxide reduction of manganese phases under oxygen-deficient conditions, to produce residual  $\text{Cu}_2\text{O}$  and  $\text{Mn}^{2+/3+}$  oxide phases [17,24]. The success of  $\text{CuMnO}_x$  mixed oxide catalyst has prompted a big deal of fundamental work devoted to instructive the role played by each element and the nature of active sites [18,25]. A better tool for  $\text{CuMnO}_x$  catalyst performance for CO oxidation is to report the activation energy for the process. The activation energy data are enviable for the modeling and designing of the catalytic converter [15,26]. The chemical kinetics establishes the factors, which influence the rate of reaction under consideration and it provides clarification for the measured value of rate and leads to the rate of equations, which are valuable in reactor design [27].

The small amounts of promoters are added into the hopcalite catalyst; has improved their catalytic performance for CO oxidation reactions at a low temperature. The existence of active species of copper in the  $\text{CuMnO}_x$  catalyst makes a strong interaction with manganese;

therefore, it has made to be more oxygen vacancy on the surface of catalyst [18]. In the present study, we have prepared a  $\text{CuMnO}_x$  catalyst and it's calcined by different methods like stagnant air, flowing air and reactive calcination conditions. The preparation of  $\text{CuMnO}_x$  has been played an important role in the performance of the final catalyst. This paper showed that the calcination of  $\text{CuMnO}_x$  catalyst by different conditions can modify the CO adsorption ability of the catalyst and thus affect the catalytic oxidation of CO. In the previous study, we have observed that the  $\text{CuMnO}_x$  catalyst is also active for CO oxidation at a long time. In the previous study Hasegawa *et al.*, Jones *et al.*, and Solsona *et al.* reported that the complete oxidation of CO by  $\text{CuMnO}_x$  catalyst at a temperature of 120, 200, and 210 °C, respectively [28-29,19].

In this article, the effect of preparation method and calcination conditions on the activity of  $\text{CuMnO}_x$  catalyst for CO oxidation has been reported. Tanaka and Co-authors also have demonstrated the total oxidation of CO by  $\text{CuMnO}_x$  spinel oxide catalyst is 210 °C temperature [30]. The surface area of  $\text{CuMnO}_x$  catalyst has highly effect on their catalytic activity and it has also discussed in this paper. According to Cai *et al.* the selection of proper precursors and precipitant prepared by the coprecipitation method is highly affected on the catalyst performance [8]. From the experimental results, we can get that the  $\text{CuMnO}_x$  catalyst prepared by reactive calcination conditions is more active for the complete oxidation of CO as compared to stagnant air and flowing air calcination prepared  $\text{CuMnO}_x$  catalyst.

## 2. Experimental

### 2.1 Catalyst preparation

The amorphous manganese oxide (AMO) catalyst was prepared by the reduction of potassium permanganate ( $\text{KMnO}_4$ ) with manganese(II) acetate tetra hydrate (of Mn  $(\text{CH}_3\text{COO})_2 \cdot 4\text{H}_2\text{O}$ ). A solution of Mn  $(\text{CH}_3\text{COO})_2 \cdot 4\text{H}_2\text{O}$  (14.70 g in 33 mL  $\text{H}_2\text{O}$ ) was added drop wise to a solution of  $\text{KMnO}_4$  (6.32 g in 33 mL  $\text{H}_2\text{O}$ ) under vigorous stirring conditions. The resultant precipitate was stirred con-

tinuously for 4 h, filtered, washed, vacuum dried, and ground into powder. The above procedure was modified to prepare binary copper manganese oxides by adding 3.68 g of copper(II) nitrate ( $\text{Cu}(\text{NO}_3)_2 \cdot 2.5\text{H}_2\text{O}$ ) to the manganese(II) acetate solution before reduction. The resulting precipitate was stirred continuously for 2 h [16]. The resulting precipitate was filtered and washed several times with ethyl alcohol and hot distilled water to remove all the impurity. The cake thus obtained was dried at different temperatures (22, 50, 90, 110, and 120 °C) for 12 h into the oven. The precursor was calcined under different conditions such as stagnant air, flowing air and reactive calcination at 300 °C for 2 h. The nomenclature of the catalysts thus obtained after calcination is given in Table 1. The catalysts prepared as above were stored in a capped glass sample holders placed in desiccators. The granules were crushed into powder and used without any further pretreatment.

### 2.2 Different calcination conditions

The catalyst precursor was calcined under the following three different conditions:

- (i) Stagnant air calcination: The calcination of the precursor was done in a furnace in the presence of stagnant air at a temperature of 300 °C for 2 h to produce the  $\text{CuMnO}_x$  catalyst. The calcined catalyst was stored in an airtight glass bottle.
- (ii) Flowing air calcination: The calcination of the  $\text{CuMnO}_x$  precursor was performed *in situ* under flowing air in the reactor at 300 °C for 2 h, just before the activity measurement experiment.
- (iii) Reactive calcination: The calcination of the  $\text{CuMnO}_x$  precursor was performed *in situ* under a flowing reactive mixture of 4.5% in CO-air at 300 °C for 2 h, just before the activity measurement experiment.

### 2.3 Characterization

The X-ray diffraction (XRD) measurement of the catalyst was carried out by using Rigaku D/MAX-2400 diffractometer with Cu-K $\alpha$  radiation at 40 kV and 40 mA. The mean crystallite size (*d*) of the catalyst was calculated from the

**Table 1.** Calcination strategy and nomenclature of the catalysts  $\text{CuMnO}_x$  thus obtained

Calcination Strategy	Calcination method	Nomenclature
Stagnant air calcination	Furnace	$\text{CuMn}_{\text{SA}}$
Flowing air calcination	<i>In situ</i>	$\text{CuMn}_{\text{FA}}$
Reactive calcination	<i>In situ</i>	$\text{CuMn}_{\text{RC}}$

line broadening of the most intense reflection using the Scherrer Equation. It provides information about the structure, phase, crystal orientation, lattice parameters, crystallite size, strain and crystal defects, etc. The Fourier transform infrared spectroscopy (FTIR) analysis was done by Shimadzu 8400 FTIR spectrometer in the range of 400-4000  $\text{cm}^{-1}$ . It provides information about the kind of materials present in a catalyst sample by their peak values. The Scanning electron micrographs (SEM-EDX) produced the topographical image of a catalyst by an electron beam and the image of catalyst was recorded on Zeiss EVO 18 (SEM) instrument. The accelerating voltage was used 15 kV and magnification of the image was 5000X applied. It provides information about the average aggregate size, crystallinity degree and the microstructures of the catalyst. The X-ray Photoelectron Spectroscopy (XPS) analysis of the catalyst was measured with Amicus spectrometer equipped with Al-K $\alpha$  X-ray radiation at a voltage of 15 kV and current of 12 mA. It provides information about the surface compositions and chemical states of the different constituent elements present in a catalyst. The Brunauer-Emmett-Teller (BET) analysis provides information about the specific surface area, pore size and pore volume of the catalyst. The isotherm was recorded by Micromeritics ASAP 2020 analyzer and the physical adsorption of N<sub>2</sub> at the temperature of liquid nitrogen (-196 °C) with a standard pressure range of 0.05-0.30 P/P<sub>0</sub>.

#### 2.4 Catalytic Activity Measurement

The oxidation of CO was carried out under the following reaction conditions, 100 mg of catalyst with feed gas consisting of a lean mixture of (2.5 vol.% CO in air) and the total flow rate was maintained at 60 mL/min. The air feed into the reactor was made free from moisture and CO<sub>2</sub> by passing through it CaO and KOH pellet drying towers. The catalytic experi-

ment was carried out under the steady state conditions and the reaction temperature was increased from room temperature to 200 °C with a heating rate of 1 °C/min. To monitor the flow rate of CO and air through the catalyst in the presence of a reactor was done by digital gas flow meters. For controlling the heating temperature of catalyst presence in a reactor was done by a microprocessor based temperature controller. The gaseous products were produced after the oxidation reaction in a reactor was analysis by an online gas chromatogram (Nucon series 5765) equipped with a Porapak Q-column, FID detector, and a methaniser for measuring the concentration of CO and CO<sub>2</sub>. The oxidation of CO at any instant was calculated on the basis of concentration CO in the feed and product stream by equations (1).

$$(X_{CO}) = \frac{[(C_{CO})_{in} - (C_{CO})_{out}]}{[(C_{CO})_{in}]} = \frac{[(A_{CO})_{in} - (A_{CO})_{out}]}{[(A_{CO})_{in}]} \quad (1)$$

where, the concentration of CO was proportional to the area of chromatogram  $A_{CO}$ . The overall concentration of CO in the inlet stream was proportional to the area of CO<sub>2</sub> chromatogram.

### 3. Results and Discussion

#### 3.1 Catalyst characterization

The characterization of CuMnO<sub>x</sub> catalyst reveals the morphology, surface area, surface structure, phase identification, and material identification, etc.

##### 3.1.1 Morphology of the catalysts

The textures property of the catalysts was analyzed by scanning electron microscopy (SEM). The SEM micrographs of catalysts formed under three different calcination strategies (Figures 1 A, B, C) show clearly large differences in the microstructure and morphology of the porous CuMnO<sub>x</sub>. They all show granular

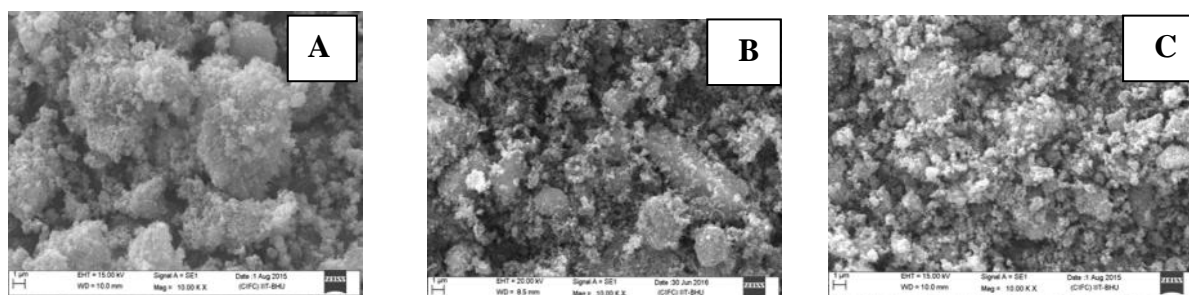


**Figure 1.** SEM image of CuMnO<sub>x</sub> catalyst produced in A) Stagnant air, B) Flowing air, and C) Reactive calcinations

particles between 5 and 10 nm calculated by “image j software” with varying degree of agglomeration.

As observed in the SEM micrograph, the particles were comprised, coarse, fine and finest size grains resulted by calcination in stagnant air, flowing air and in reactive calcinations respectively. Particles of the catalyst in calcination conditions are less agglomerated, porous and homogeneous as compared to other two samples. The size of particles presence in catalyst produced by stagnant air calcination is relatively very large and agglomerated than the catalyst in flowing air as well as in reactive calcination. The size of particles in CuMn<sub>SA</sub> catalyst is coarse, more agglomerated, less-porous and non-uniform. The structure of catalyst-CuMn<sub>FA</sub> is less agglomerated than catalyst-CuMn<sub>SA</sub>. The particles of catalyst-CuMn<sub>RC</sub> are least agglomerated, highly porous, high surface area and uniformly distributed. Thus, the different calcination conditions followed in the present study considerably affect the porosity, particle size, and morphology of the resulting catalysts.

### 3.1.2 Elemental analysis

After the SEM micrographs are taken, the elemental mapping is performed to determine the elemental concentration distribution of the catalyst granules by using Isis 300 software. It is clear from the results of the SEM-EDX analysis that all the catalysts samples were pure due to the presence of their relevant ele-

mental peaks only. The SEM-EDX analysis is performed on different cross-sectioned marks of CuMnO<sub>x</sub> catalysts granules to determine the concentration of copper, manganese, and oxygen at different locations on the CuMnO<sub>x</sub> catalysts granular surfaces as shown in Figure 2. It is very clear from the table and figures that the atomic percentage and weight percentage of Mn are also higher as the comparison of Cu and O.

In the reactive calcined prepared CuMnO<sub>x</sub> catalyst, there are three elements of Cu, Mn, and O present and shown in the Figure 2C. In Table 2 the atomic ratio and weight ratio of the Cu, Mn, and O in CuMnO<sub>x</sub> catalysts resultant in different calcination conditions are listed.

The atomic percentage of Cu, Mn, and O in the catalyst resulted by RC is 47.82%, 48.05%, and 4.13% respectively. The weight percentage of Cu, Mn, and O in this catalyst is 46.70%, 47.06%, and 6.24%, respectively. In the flowing air calcined condition also same three elements Cu, Mn, and O peaks are present as shown in the Figure 2B. The atomic percentage of Cu, Mn, and O in the CuMnO<sub>x</sub> catalyst resulted by FAC is 36.35%, 53.65%, and 10.0% respectively. The weight percentage of Cu, Mn, and O in this catalyst is 35.85%, 54.11%, and 10.04% respectively. In the stagnant air calcined conditions three elements Cu, Mn, and O are present as shown in Figure 2A. The atomic percentage of Cu, Mn, and O in the catalyst resulted by SAC is 29.39%, 57.46%, and 13.15% respectively. The weight percentage of Cu, Mn,

**Table 2.** The atomic and weight ratios of Cu, Mn, and O in CuMnO<sub>x</sub> catalyst by EDX analysis

Catalyst	Atomic ratio (%)				Weight ratio (%)			
	Cu	Mn	O	Cu/Mn	Cu	Mn	O	Cu/Mn
CuMn <sub>RC</sub>	47.82	48.05	4.13	0.995	46.70	47.06	6.24	0.993
CuMn <sub>FA</sub>	36.35	53.65	10.0	0.676	35.85	54.11	10.04	0.662
CuMn <sub>SA</sub>	29.39	57.46	13.15	0.511	29.45	57.91	12.64	0.508

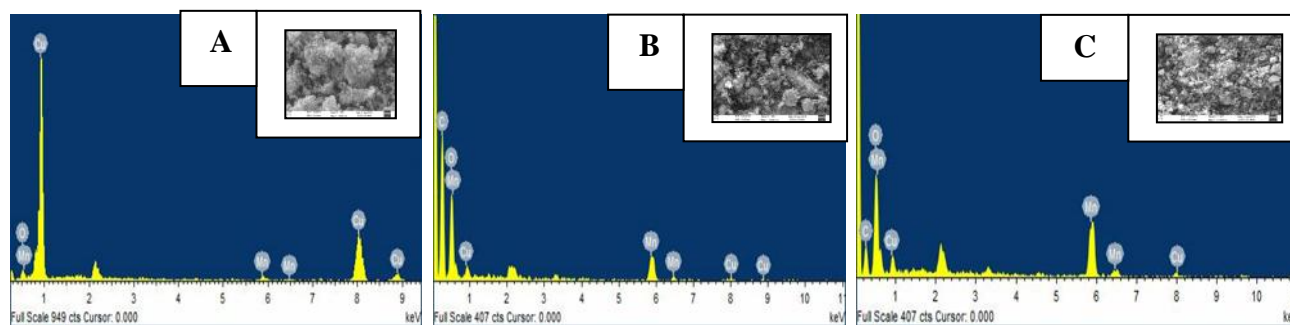


**Figure 2.** EDX image of CuMnO<sub>x</sub> catalyst produced in A) Stagnant air, B) Flowing air, and C) Reactive calcinations

and O in this catalyst is 29.45%, 57.91%, and 12.64% respectively. This presence of oxygen deficiency in the CuMn<sub>RC</sub> catalyst which makes the high density of active sites, therefore, it has shown the best catalytic activity. The Cu, Mn, and O present in the CuMnO<sub>x</sub> catalyst is easily detected by EDX analysis. The Cu/Mn atomic ratio of the CuMn<sub>RC</sub> catalyst is approximately 0.995 and the Cu/Mn weight ratio in the CuMn<sub>RC</sub> catalyst is approximately 0.993.

### 3.1.3 Phase identification and cell dimensions

The phase identification and cell dimensions of CuMnO<sub>x</sub> catalyst in different calcination conditions were done by the X-ray powder diffraction (XRD) technique. The diffraction pattern of the catalysts is represented in Figure 3.

The XRD pattern of the CuMn<sub>SA</sub> sample (Figure 3) shows that the stagnant air calcined particles consist of CuMn<sub>2</sub>O<sub>4</sub> were the crystalline major phase. The diffraction peak at 2θ of 43.95 corresponds to lattice plane (111) of face-centered cubic CuMn<sub>2</sub>O<sub>4</sub> (PDF-32-0429 JCPDS file). The crystallite size of the catalyst is 4.70 nm. In the flowing air calcination of the sample (CuMn<sub>FA</sub>) was found that resulting Cu<sub>1.2</sub>Mn<sub>1.8</sub>O<sub>4</sub> in a crystalline phase. The diffraction peak at 2θ of 37.20 corresponds to lattice plane (222) of face-centered cubic Cu<sub>1.2</sub>Mn<sub>1.8</sub>O<sub>4</sub> (PDF-71-1144 JCPDS file). The crystallite size of the catalyst is 3.28 nm. In contrast, the XRD pattern of the CuMn<sub>RC</sub> sample was quite different from those of CuMn<sub>SA</sub> and CuMn<sub>FA</sub> sample.

It shows that the well crystalline phase was CuMnO<sub>2</sub>. The diffraction peak at 2θ of 36.96 corresponds to lattice plane (222) of end centered cubic CuMnO<sub>2</sub> (PDF-75-1010 JCPDS file). The crystallite size of the catalyst is 2.71 nm. The refinement of the XRD pattern of the CuMn<sub>RC</sub> sample shows that there will be no impurity phases were present in the catalyst. The XRD data was further refined in order to gain more structural information on the CuMnO<sub>x</sub> phase's presence in the catalyst.

### 3.1.4 Identification of the materials

The FTIR transmission spectra of the CuMnO<sub>x</sub> catalysts are shown in Figure 4. In the invested region (4000-500 cm<sup>-1</sup>) to obtain the entire absorption spectra peaks to indicates the presence of different elemental groups in all the samples of the CuMnO<sub>x</sub> catalysts.

The different peak was shown different types of chemical groups present in the CuMnO<sub>x</sub> catalysts. The main four peaks were obtained in CuMnO<sub>x</sub> catalyst prepared by RC conditions. The MnO<sub>2</sub> vibration mode was observed at (1640 cm<sup>-1</sup>) due to stretching of the Mn–O bond. The transmission spectra at (532 cm<sup>-1</sup>) were assigned to CuO group. The other phases like CO<sub>3</sub><sup>2-</sup> and C=O are present at (1300 and 2350 cm<sup>-1</sup>), respectively. The main five peaks were obtained in CuMnO<sub>x</sub> catalyst prepared by SAC. The main stretching bond Mn–O, CuO, CO<sub>3</sub><sup>2-</sup> and C=O group was also present in this catalyst. The transmission spec-

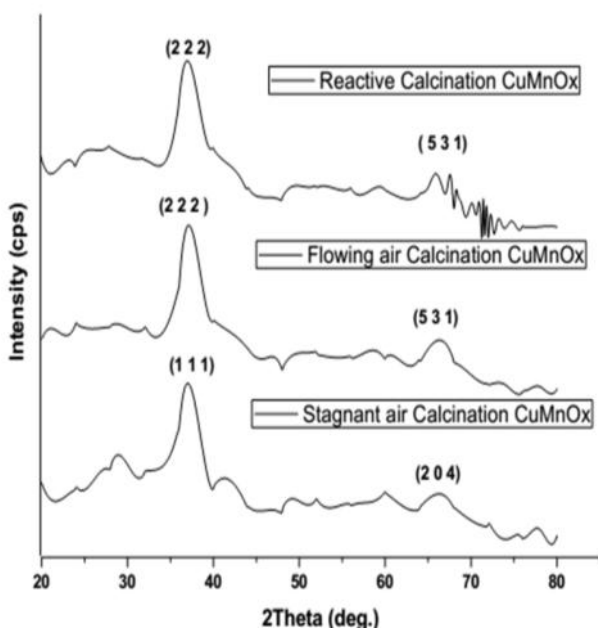


Figure 3. XRD analysis of CuMnO<sub>x</sub> catalyst in different calcination conditions

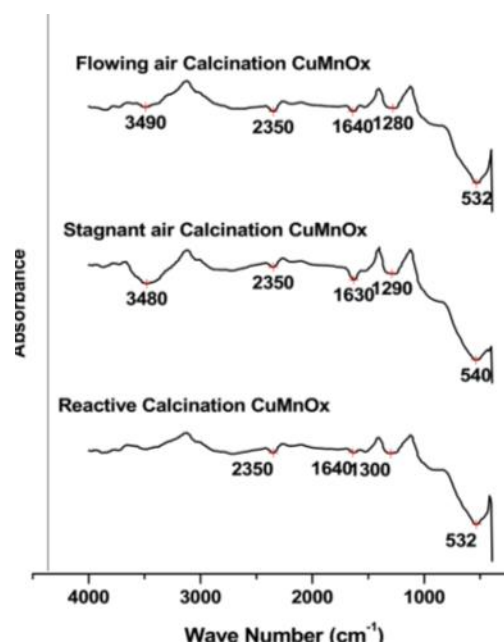


Figure 4. FTIR analysis of CuMnO<sub>x</sub> catalyst in different calcination conditions

trum at (1630  $\text{cm}^{-1}$ ) has show  $\text{MnO}_2$  group, (1290  $\text{cm}^{-1}$ ) show  $\text{CO}_3^{2-}$  group and (540  $\text{cm}^{-1}$ ) was assigned to  $\text{CuO}$  group. The other phases, like  $\text{C}=\text{O}$  and hydroxyl group, are present at (2350  $\text{cm}^{-1}$  and 3480  $\text{cm}^{-1}$ ), respectively.

The FTIR analysis of  $\text{CuMnO}_x$  catalyst prepared by FAC conditions they were five peaks we obtained. The transmission spectra at (1640  $\text{cm}^{-1}$ ) show  $\text{MnO}_2$ , (1280  $\text{cm}^{-1}$ ) show  $\text{CO}_3^{2-}$  group, (2350  $\text{cm}^{-1}$ ) shows  $\text{C}=\text{O}$  presence, (3490  $\text{cm}^{-1}$ ) show hydroxyl group, and (532  $\text{cm}^{-1}$ ) shows  $\text{CuO}$  group presence. The spectra of impurities like hydroxyl group at 3480  $\text{cm}^{-1}$  decreases in the following the order:  $\text{CuMn}_{\text{SA}} > \text{CuMn}_{\text{FA}} > \text{CuMn}_{\text{RC}}$ . Thus  $\text{CuMn}_{\text{RC}}$  is highly pure as compare to  $\text{CuMn}_{\text{FA}}$  and  $\text{CuMn}_{\text{SA}}$ . All the sample of  $\text{CuMnO}_x$  catalysts; which originates from the stretching vibrations of the metal-oxygen bond and confirm the presence of  $\text{CuO}$  and  $\text{MnO}_2$  phases.

### 3.1.5 Identification and quantification of elements

The oxidation state and atomic concentration of  $\text{Cu-Mn}$  mixed oxide investigated by X-ray photoelectron spectroscopy (XPS) analysis. The XPS analysis is mainly used to understand the physical and chemical changes by exposure of gaseous molecule under different thermal conditions examined. Although it can be proposed that the high binding energy is preferably for the oxidation reaction. The Figures 5, 6, and 7 displayed the spectra in the  $\text{Cu}(2p)$ ,  $\text{Mn}(2p)$  and  $\text{O}(1s)$  regions. The XPS spectra of  $\text{Cu}(2p)$  region is presented in Figure 5. By performing peak fitting deconvolution the main  $\text{Cu}_{p_{3/2}}$  in all three calcination catalyst is  $\text{Cu(II)}$  oxide form. The binding energy of  $\text{Cu}(2p)$  in  $\text{CuMnO}_x$  catalyst is stagnant air, flowing air

and reactive calcinations condition is 935.8 eV, 934.2 eV and 936.5 eV, respectively. In Figure 5, we have observed that the prominent peak of  $\text{Cu}(2p)$  level in  $\text{CuMnO}_x$  catalyst is deconvoluted into five peaks centered and the highest binding energy were found in  $\text{CuMn}_{\text{RC}}$  catalyst is 936.5 eV. It is very clear from the table and figure that the binding energy of  $\text{Cu}(2p)$  in  $\text{CuMnO}_x$  catalyst is highest in RC preparation conditions as compared to flowing air and stagnant air prepared a catalyst.

The XPS spectra in the  $\text{Mn}(2p)$  region is presented in Figure 6. By performing peak fitting deconvolution the main  $\text{Mn}_{p_{3/2}}$  in all three calcination catalyst is  $\text{MnO}_2$  form. In the Figures 6 and 7 the prominent peak of  $\text{Mn}(2p)$  level and  $\text{O}(1s)$  level in  $\text{CuMnO}_x$  catalyst is deconvoluted into double and single peak respectively. By performing peak fitting deconvolution the main  $\text{Mn}(2p)$  in all the three samples can be divided into three components including  $\text{Mn}^{4+}$ ,  $\text{Mn}^{3+}$ , and satellite. Since the differences between the binding energy values of  $\text{Mn}^{3+}$  and  $\text{Mn}^{4+}$  ions are small. The observed of  $\text{Mn}(2p)$  in  $\text{CuMnO}_x$  catalyst is stagnant air, flowing air, and reactive calcinations condition is 640.6 eV, 641.2 eV, and 641.8 eV, respectively and it will be associated with the presence of  $\text{Mn}^{3+}$ ,  $\text{Mn}^{4+}$ , and satellite in all the three samples.

From the Figure 6, the broad  $\text{Mn}^{4+}$  peak is presented in  $\text{CuMn}_{\text{RC}}$  which indicated that the composition of  $\text{Mn}^{4+}$  is higher than  $\text{CuMn}_{\text{FA}}$  and  $\text{CuMn}_{\text{SA}}$ . It is very clear from the figure that the binding energy of  $\text{Mn}(2p)$  in  $\text{CuMnO}_x$  catalyst is highest in RC preparation conditions as compared to flowing air and stagnant air prepared a catalyst. The binding energy of  $\text{O}(1s)$  is display in Figure 7(C). Generally, there are two different types of oxygen present in the catalysts with binding energy of (529.2-

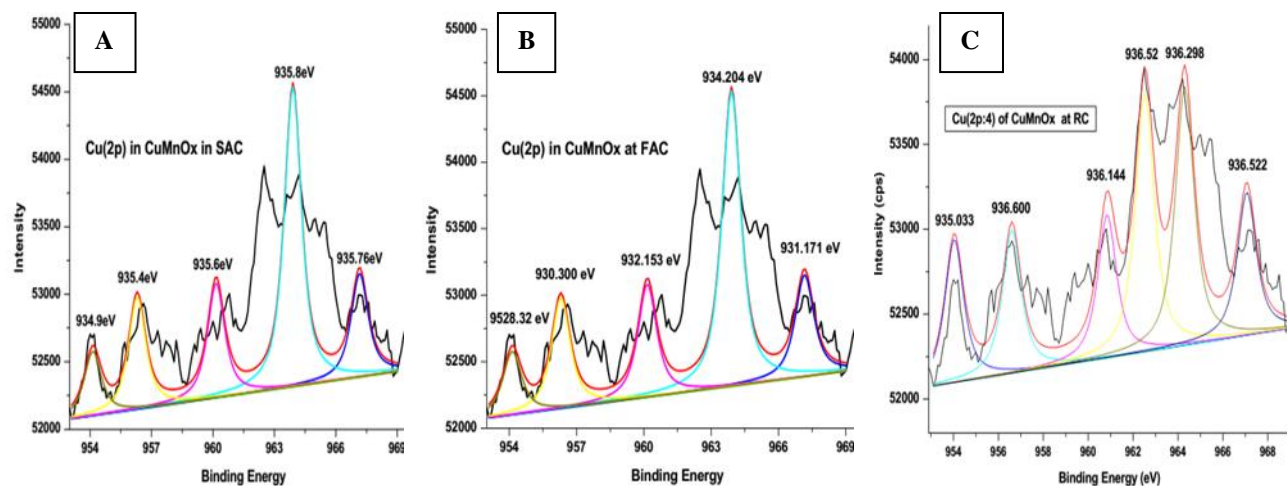


Figure 5. XPS analysis of  $\text{Mn}(2p)$  in  $\text{CuMnO}_x$  catalysts: A)  $\text{CuMn}_{\text{SA}}$ , B)  $\text{CuMn}_{\text{FA}}$ , and C)  $\text{CuMn}_{\text{RC}}$

530 eV) and (531.3-532.2 eV), which could be recognized as chemisorbed oxygen (denoted as  $O_a$ , such as:  $O_2^{2-}$ ,  $O^-$ ,  $OH^-$ ,  $CO_3^{2-}$ , etc.) and lattice oxygen (denoted as  $O_l$ , such as  $O^{2-}$ ), respectively. In our case, oxygen with the binding energy of 530.8 eV was the main form and could be assigned to the chemisorbed oxygen ( $O_a$ ). The presence of lattice oxygen is very small in  $CuMn_{RC}$ . The binding energy of  $O(1s)$  in  $CuMn_{RC}$ ,  $CuMn_{FA}$ ,  $CuMn_{SA}$  catalyst is 529.8 eV, 530.50 eV and 530.8 eV, respectively and the presence of lattice oxygen is very small in reactive calcined prepared  $CuMnO_x$  catalyst.

Tables 3 and 4 represent the chemical state and binding energy of  $CuMnO_x$  catalyst in different calcination conditions. It is confirmed that  $Mn(CH_3COO)_2 \cdot 4H_2O$  is usually decomposed into  $MnO_2$  and  $Cu(NO_3)_2 \cdot 3H_2O$  is usually decomposed into  $Cu(II)$  oxide after calcination in different conditions like stagnant air, flowing air and reactive calcination conditions. The binding energy of  $CuMn_{RC}$  catalyst is highest as the comparison to  $CuMn_{FA}$  and  $CuMn_{SA}$  catalyst. One of noticeable fact is that the amount of

oxygen present is less in reactive calcined prepared  $CuMnO_x$  catalyst as compared to flowing air and stagnant air prepared  $CuMnO_x$  catalyst due to an absence of lattice oxygen which creates oxygen vacancies for oxidation reactions.

The content order of  $O_a/(O_a + O_l)$  ratio was shown as following:  $CuMn_{RC} > CuMn_{FA} > CuMn_{SA}$ . The high amount of chemisorbed oxygen is preferable for increasing the  $CuMnO_x$  catalyst activity of CO oxidation reactions. The extraordinary performance of  $CuMn_{RC}$  catalyst produced by RC in CO oxidation is associated with their characterizations such as physical and chemical changes, binding energy and oxygen deficient defective structure which create the high density of active sites. So, RC route can be recommended for the synthesis of highly active catalysts. The presence of higher oxidation state phases could be the result of a greater degree of surface interaction between the easily oxidisable manganese phase and the highly reducible copper phase.

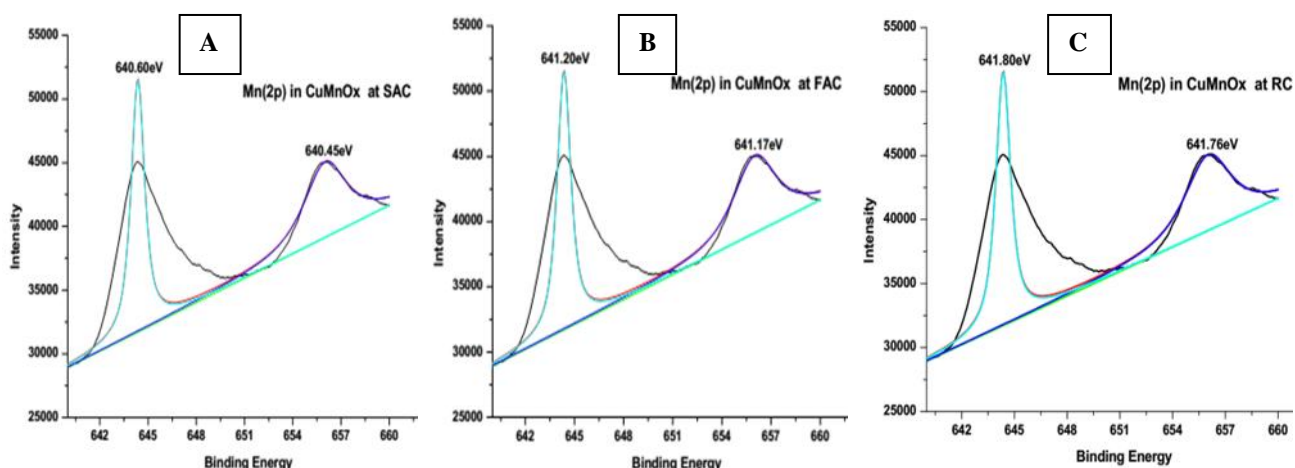


Figure 6. XPS analysis of Mn(2p) in  $CuMnO_x$  catalysts A)  $CuMn_{SA}$ , B)  $CuMn_{FA}$  and C)  $CuMn_{RC}$

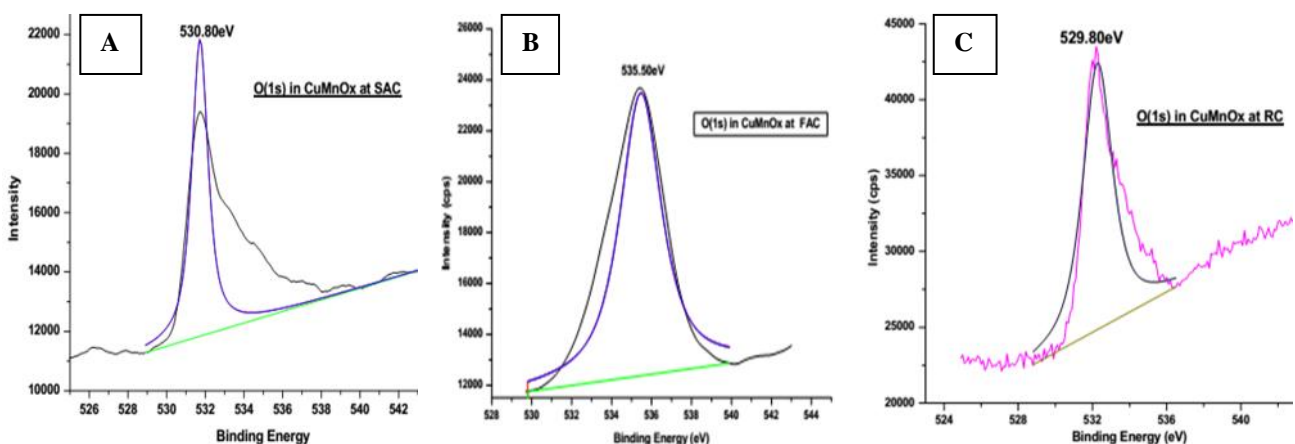


Figure 7. XPS analysis of  $O(1s)$  in  $CuMnO_x$  catalysts A)  $CuMn_{SA}$ , B)  $CuMn_{FA}$  and C)  $CuMn_{RC}$

In addition, the interaction between the copper and manganese phases during decomposition facilitates the formation of stable metal oxide interfaces. These XPS results suggest that the most active catalyst (CuMn<sub>RC</sub>) had a relatively higher amount of lower valence manganese and loosely bound lattice oxygen. The presence of binding energy in CuMnO<sub>x</sub> catalyst as follows: CuMn<sub>RC</sub> > CuMn<sub>FA</sub> > CuMn<sub>SA</sub>. In the activity test, we have found out that the performance of CuMnO<sub>x</sub> catalysts for CO oxidation is in accordance with their characterization.

### 3.1.6 Surface area measurement of catalyst

The surface area of CuMnO<sub>x</sub> catalyst prepared by the precipitation method with a novel route in reactive calcination (267.80 m<sup>2</sup>/g) is much superior to those of the catalysts prepared by other calcination routes like flowing air (210.50 m<sup>2</sup>/g) and stagnant air (165.40 m<sup>2</sup>/g). It can be visualized from the Table 5 that the textural property of CuMnO<sub>x</sub> catalyst in reactive calcined are higher than other two catalyst samples of CuMn<sub>FA</sub> and CuMn<sub>SA</sub>. The isotherm gave useful information on the mesopore structure through its hysteresis loop. The prepared samples exhibited hysteresis loop, which indicated that the pores were exhibiting geometries of mesopores. The effect of different calcination conditions on the isotherms of CuMnO<sub>x</sub> catalyst. The specific surface area of CuMnO<sub>x</sub> catalyst is measured by BET and it also follows the SEM and XRD results.

The specific surface area and total pore volume were two main factors for the effect on the CuMnO<sub>x</sub> catalyst performance for CO oxidation reactions. The surface area and average pore

diameter increased with the increasing of calcination temperature because a high-temperature treatment led to particle sintering therefore a loss in the active area. The larger number of more pores presence in a CuMnO<sub>x</sub> catalyst surfaces means a higher number of CO molecules capture on their surfaces, therefore, it shows better catalytic activity.

## 3.2 Catalyst Activity

### 3.2.1 Optimization of drying temperature of precursor on resulting catalyst for CO oxidation

The performance of CuMnO<sub>x</sub> catalysts was carried out to compare the efficiency of catalysts produced by drying the precursor at different temperatures (22-120 °C) followed by RC for CO oxidation. It can be seen from the Figure 8 that the activity of CuMnO<sub>x</sub> catalysts increase with the increasing of drying temperature up to 110 °C, with further increasing the temperature the activity of the catalyst was decreased.

Thus, the optimum drying temperature of CuMnO<sub>x</sub> precursor is 110 °C, which produced catalyst exhibiting the highest activity for 100% CO conversion at 80 °C. The light of characteristics for the different drying temperature of CuMnO<sub>x</sub> precursor which is tabulated in Table 6 and it's used to evaluate the activity of resulting catalyst. The characteristic temperature T<sub>10</sub>, T<sub>50</sub>, and T<sub>100</sub> corresponds to the initially, half and complete oxidation of CO respectively. The activity of final catalyst increases with the increasing of precipitate drying temperature and in the activity test, we

**Table 3.** Chemical state of CuMnO<sub>x</sub> catalysts in XPS analysis

Sample	Elements			
	C	Cu	Mn	O
CuMn <sub>RC</sub>	C–O–C	Cu(II) oxide	MnO <sub>2</sub>	Organic C–O
CuMn <sub>FA</sub>	C–O–C	Cu(II) oxide	MnO <sub>2</sub>	Organic C–O
CuMn <sub>SA</sub>	C–O–C	Cu(II) oxide	MnO <sub>2</sub>	Organic C–O

**Table 4.** The binding energy of CuMnO<sub>x</sub> catalysts in XPS analysis

Sample	Elements (eV)		
	Cu	Mn	O
CuMn <sub>RC</sub>	936.5	641.8	529.8
CuMn <sub>FA</sub>	934.2	641.2	530.5
CuMn <sub>SA</sub>	935.8	640.6	530.8

have got the optimum drying temperature, of CuMnO<sub>x</sub> catalyst. From the table and figure, it is considered to be the 110 °C maximum possible operating temperature of CuMnO<sub>x</sub> catalyst for CO oxidation.

During the drying period, the CuMnO<sub>x</sub> solution may be retained by the porous support, and it may be migrated by capillary flow and diffusion, therefore; the solute redistributed by desorption and re-adsorption. When the solvent evaporates, precipitation of solute happens as the solution becomes supersaturated and brings crystallization of the CuMnO<sub>x</sub> precursors in the pores and an outer surface of the carrier. The solvent is removing during the drying process, and the concentration of precursor will raise therefore the critical supersaturating, precipitation will take place. The uniform drying of CuMnO<sub>x</sub> precursor reduces the convection so that more similar distributions are obtained in a catalyst.

### 3.2.2 Performance of CuMnO<sub>x</sub> catalyst for CO oxidation at different calcination conditions

Reactive calcination of CuMnO<sub>x</sub> precursor was carried out by passing a CO-Air mixture over the precursors at 160 °C temperature for some time then increased the temperature up to 300 °C. In the beginning, the limited rise in the temperature of precursor's crystallites due to very slow exothermic oxidation which ensures very slow decomposition of the precursor. Then after, slightly faster CO oxidation was ob-

served. The effect of calcination strategies of the precursor on the produced catalysts towards CO oxidation is shown in Figure 9. A comparison of light-off temperatures of all the catalysts produced by RC and traditional way of calcination are given in Table 7. It is quite evident from the figure and table that the oxidation of CO was initiated at 25, 45, and 55 °C over CuMn<sub>R</sub>C, CuMn<sub>F</sub>A, and CuMn<sub>S</sub>A respectively. The total oxidation temperature of CO is 80 °C for CuMn<sub>R</sub>C, which was less by 40 °C and 80 °C than that of CuMn<sub>F</sub>A and CuMn<sub>S</sub>A respectively. The improved catalytic activity of CuMnO<sub>x</sub> (R.C.) can be ascribed to the distinc-

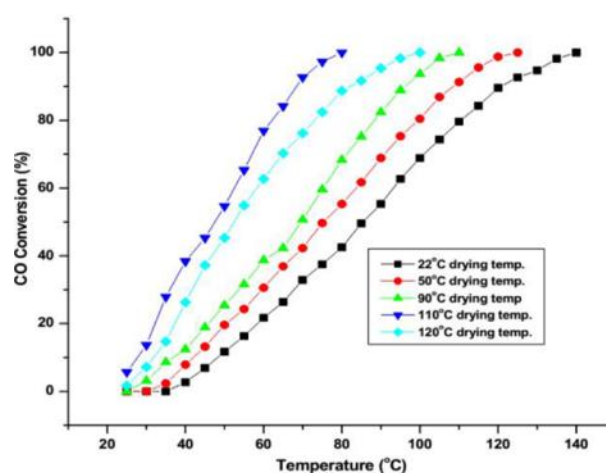


Figure 8. Effect of drying temperature on CuMn<sub>R</sub>C catalyst for CO oxidation

Table 6. Light-off temperature (L.O.T) at different drying temperature

Drying temperature of CuMnO <sub>x</sub> catalyst (°C)	T <sub>10</sub> (°C)	T <sub>50</sub> (°C)	T <sub>100</sub> (°C)
22	50	85	140
50	40	75	125
90	35	70	110
110	30	48	80
120	35	55	100

(T<sub>10</sub>= 10% conversion, T<sub>50</sub>= 50% conversion, T<sub>100</sub> = 100% conversion of CO)

Table 5. The surface area, pore volume and pore size of CuMnO<sub>x</sub> catalyst in different calcination conditions

Catalyst	Surface Area (m <sup>2</sup> /g)	Pore Volume (cm <sup>3</sup> /g)	Average Pore Size (Å)
CuMn <sub>R</sub> C	267.80	0.640	78.60
CuMn <sub>F</sub> A	210.50	0.460	52.30
CuMn <sub>S</sub> A	165.40	0.310	32.55

tive structural and textural characteristics such as the smallest crystallites of CuMn<sub>RC</sub>, highly dispersed and highest specific surface area with oxygen deficient crystallite structure which could expose more active sites for CO oxidation. Further, relatively open textured pores of the catalyst favor easy diffusion of reactants and products and thus facilitate the oxidation process.

It is apparent from the Figure 9 that the CuMnO<sub>x</sub> catalyst produced by following the novel route of RC of the precursors is more active for CO oxidation than the ones prepared by the traditional method of calcination of the same precursors in air. As the calcination conditions of stagnant air and flowing air affect the activity of resulting catalyst and Figure 9 also shows the comparison of CuMn<sub>F</sub>A produced by calcination in flowing air with CuMn<sub>S</sub>A and CuMn<sub>RC</sub>. It is very clear from Figure 9 that the activity of CuMn<sub>F</sub>A lies in between the activities of CuMn<sub>S</sub>A and CuMn<sub>RC</sub>. From the table and figure, we get that RC produced catalysts are more active than catalysts produced by conventional methods of calcination, whether it is in stagnant or flowing air. Thus, the activity order of catalysts obtained by various calcinations methods is as follows: RC > flowing air > stagnant air. The reason for the high activity of RC produced catalysts as compared to catalysts obtained by traditional calcination methods may be due to the combined effect of phases, high surface area, and smallest crystalline size.

The novelty of CuMnO<sub>x</sub> catalyst produced by RC is associated with the presence of nano-sized major phases and usual morphology. The improved catalytic activity of CuMn<sub>RC</sub> can be ascribed to the unique structural and textural characteristics as the smallest crystallites of CuMn<sub>RC</sub>, highly dispersed and highest specific surface area which could expose more active sites for catalytic oxidation and relatively open textured pores which will favor for the adsorption of reactants and desorption of products and thus facilitate the oxidation process. Moreover, the presence of partially reduced phase provides an oxygen deficient defective structure which creates a high density of active sites as a

result of reactive calcination, consequently CuMn<sub>RC</sub> turn into the most active catalyst.

The reactive calcination technique could be extended and expanded to provide a convenient strategy for the synthesis of oxide structures for several reactions in a single step minimizing the drawbacks of the conventional methods of two-step processes of calcination and activation. The high precision of EDX measurements and the morphological uniformity of the samples (examined by SEM) suggest that the elemental composition of CuMn<sub>RC</sub> synthesized using the redox method is homogeneous and it will be the major factors contributing to their high catalytic activity. The activity order of CuMnO<sub>x</sub> catalysts produced by different calcination conditions is in accordance with their characterization. Therefore, we can be summarized that the calcination strategies of precursor have great influence on the activity of resulting catalysts.

### 3.3 Kinetics study of CuMnO<sub>x</sub> catalyst

The significant kinetic data can be obtained from a packed bed reactor, only if the flow pattern within the reactor resembles plug flow. In the present study, the different concentration of CO present in air flows through the CuMn<sub>RC</sub> catalyst as shown in Figure 10. In the experiments, we have taken 100 mg of the catalyst

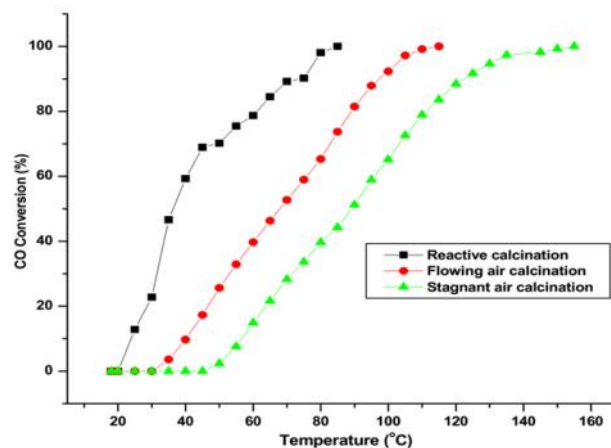


Figure 9. The activity of CuMnO<sub>x</sub> catalyst prepared in different calcination conditions

Table 7. Light-off Temperature (L.O.T.) at different calcination conditions

Calcinations of CuMnO <sub>x</sub> Catalyst	T <sub>10</sub> (°C)	T <sub>50</sub> (°C)	T <sub>100</sub> (°C)
CuMn <sub>RC</sub>	25	40	80
CuMn <sub>F</sub> A	45	70	120
CuMn <sub>S</sub> A	55	90	160

with CO flow rate (0.5-1.75 mL/min) and air flow rate (58.25-59.5 mL/min). The total flow rate (CO+Air) was maintained at 60 mL/min at the room temperature.

The conversion of CO is highly depending on the catalyst temperature. It is important to determine the catalyst bed temperature gradients. The comparison of inlet and bed temperature for all the runs and the axial bed temperature profiles of selected runs showed that under most operating conditions, the reactor is sufficiently isothermal for this study.

The CO conversion is measured at the time on stream of 120 min (after the reactant gasses are introduced into the system), which should be sufficient to reach the steady state conditions. In Table 8, we have observed that the CO flow rate (mL/min) at different temperature with the various CO conversion percentage. From the tables and figures, we get that (1.50 mL/min) CO flow rate in the air is the optimum flow rate of CO in the air and the complete conversion of CO at 80 °C temperature has occurred.

### 3.3.1 Weight hourly space velocity over CuMn<sub>R</sub>C catalyst

In the present study, the reaction conditions have been completely satisfied, and it implies that the reactor used behaving as an ideal plug flow reactor. The kinetic experiments repeated for feed composition at a temperature range (25-45 °C), to ensure that the data correspond to the linear change of CO conversion ( $X_{CO}$ ) with space-time ( $W/F_{CO}$ ) in the initial rates region in which the reaction is kinetically controlled. Therefore, the rate of CO oxidation in the plug flow reactor can be given as Equation 2.

$$-r_{CO} = dX_{CO}/d(W/F_{CO}) \quad (2)$$

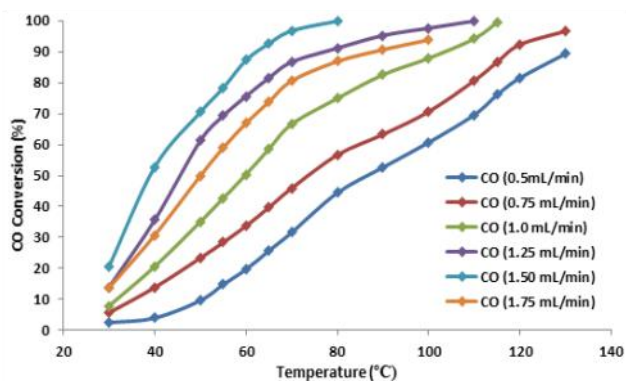


Figure 10. CO oxidation at CO (mL/min) vs temperature (°C)

where  $X_{CO}$  is the conversion of CO and  $W/F_{CO}$  is the weight hourly space velocity (WHSV). The constants in each model equations are combined as much as possible to minimize the number of unknowns and, therefore, the number of experimental data required.

Many runs in the packed bed reactor are performed applying various values of WHSV. Variation in  $W/F_{CO}$  is made by varying either catalyst weight or feed rate of CO and keeping the other parameters constant minimize the heat and mass transfer effects and to reach approximately the performance of differential reactor, the upper limit of CO conversion for each run is restricted to 15 %. The rate of reaction at any conversion can be obtained by measuring the slope on the curve, which was obtained by plotting  $X_{CO}$  versus  $W/F_{CO}$  values as shown in Figure 11 (Equation 3).

$$-r_{CO} = k (C_{CO})^n (C_{O_2})^m \quad (3)$$

where  $k$  is the reaction rate constant, and  $C_{CO}$  is the concentration of carbon monoxide, and  $C_{O_2}$  is the concentration of oxygen. In this experiment a lean mixture of reactant, 2.5 % CO in the air is used; therefore oxygen is in huge excess, and the rate of expression reduces to the pseudo  $n^{\text{th}}$  order Equation 4 or 5.

$$-r_{CO} = k(C_{CO})^n \quad (4)$$

or

$$\ln(-r_{CO}) = \ln k + n \ln C_{CO} \quad (5)$$

The data of partial conversion of  $X_{CO}$  versus  $W/F_{CO}$  at five different temperatures is shown in Figure 12. The rate of reaction ( $-r_{CO}$ ) at a different degree of conversion for each temperature is determined by measuring the slope of curves. If the power law is applicable and  $-r_{CO}$  versus  $C_{CO}$  data are recognized at the constant temperature,  $n$  and  $k$  at that temperature can be determined from a plot of  $\ln(-r_{CO})$  versus  $\ln(C_{CO})$ . The kinetic parameters ( $k$  and  $n$ ) of the power law model for the oxidation of CO are determined from the slope and intercept of the plot (Figure 13). Order of the reaction is found to be 0.84. The rate constant,  $k$ , is a function of temperature and can be expressed by Arrhenius Equation (6).

$$k = A \exp(-E/RT) \quad (6)$$

or

$$\ln k = \ln A - E/RT \quad (7)$$

The activation energy ( $E$ ) of the reaction can be evaluated from the slope of plot  $\ln(k)$  versus  $1/T$  as per Equation (9). The linear plot was ob-

tained when  $\ln(k)$  vs  $1/T$  has been plotted (Figure 13). The data of partial oxidation of CO ( $X_{CO}$ ) to  $CO_2$  under the conditions, when the catalyst exhibited steady performance, versus  $W/F_{CO}$  at five different temperatures.

The activation energy and pre-exponential factor ( $A$ ) of Arrhenius equation thus determined are given below:

$$\text{Activation energy } (E) = 8.839 \text{ kcal/gmol} = 36.98 \text{ kJ/gmol} \quad (8)$$

$$\text{Pre-exponential factor } (A) = 5.856 \times 10^5 \text{ (gmol)/(g}_{cat}\cdot\text{h)} \quad (9)$$

On the basis of experimental results, the rate of CO oxidation in the temperature ranges of 25-45 °C on the  $CuMnO_x$  catalyst can be expressed as follows:

$$-r_p = 5.856 \times 10^5 \exp(-10839/RT)(C_{CO})^{0.84} \text{ gmol/g}_{cat}\cdot\text{h} \quad (10)$$

The above empirical rate expression can be adequately used for the design of catalytic con-

verter used in automobile fuelled vehicles. The CO conversion ( $X_{CO}$ ) data taken at constant feed composition by varying space-time ( $W/F_{CO}$ ) are used to confirm the linear change characteristic of the initial rates region; the data with linear regression constants 99 % or better were

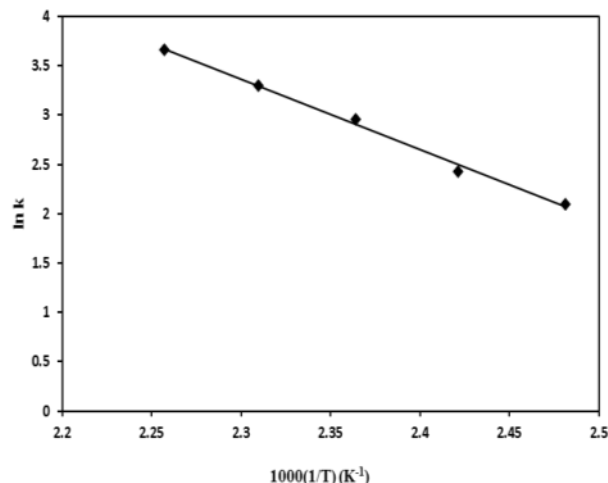


Figure 13. Arrhenius plot

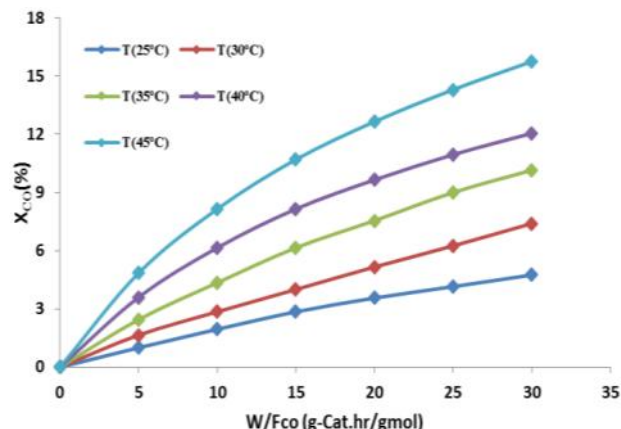


Figure 11. CO conversion,  $X_{CO}$  (%) vs  $W/F_{CO}$  ( $g_{cat}\cdot h/gmol$ ) at different temperatures

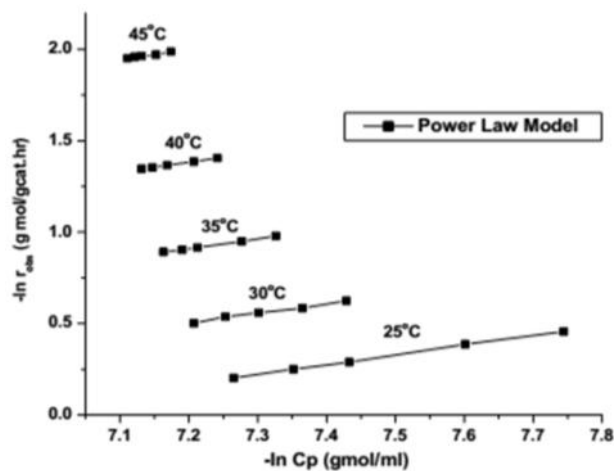


Figure 12. Plot of  $\ln(-r_{obs})$  vs  $-\ln C_P$

Table 8. The CO flow rate (mL/min) at different temperature vs conversion

CO flow rate (mL/min)	Conversion (%)				
	T <sub>30°C</sub>	T <sub>45°C</sub>	T <sub>50°C</sub>	T <sub>55°C</sub>	T <sub>60°C</sub>
0.50	0	5.40	10.35	15.35	20.30
0.75	5.65	15.80	20.35	26.35	33.70
1.00	7.85	27.75	35.08	43.36	50.65
1.25	13.90	52.70	61.30	68.65	72.70
1.50	20.65	58.60	70.30	81.65	85.95
1.75	16.70	36.70	50.90	57.60	72.70

used in the subsequent individual rate calculations. The selectivity for CO oxidation is defined as the amount of oxygen consumed in CO oxidation divided by the total amount of oxygen consumed, taking into consideration reaction stoichiometry. The kinetics of low-temperature CO oxidation on CuMnO<sub>x</sub> catalyst is investigated at (25-45 °C) over a relatively wide range of CO (2.5 mol %) concentrations. The rate of CO oxidation increases with the increasing of O<sub>2</sub> concentration. The CuMnO<sub>x</sub> catalyst used to plays an important mechanistic role in the oxidation of CO. This method provides a reasonable fit to the kinetic data from both aged catalysts.

#### 4. Conclusions

It can be concluded that the drying and calcination strategies of precursor have a great influence on the activity of resulting catalyst. The optimum drying temperature of the precursor was 110 °C. The RC route was the most appropriated calcination strategy for the production of highly active CuMnO<sub>x</sub> catalyst for oxidation of CO. The calcination orders with respect to the performance of catalysts for CO oxidation were as follows: reactive calcination > flowing air > stagnant air. The performance of CuMnO<sub>x</sub> catalyst was in accordance with the results of characterization. The extraordinary performance of CuMnO<sub>x</sub> catalyst produced by RC for CO oxidation was associated with the modification in intrinsic textural and morphological characteristics such as surface area, crystallite size, particle size, and oxygen deficient defective structure which generate the high density of active sites. So, RC route can be recommended for the synthesis of highly active catalysts. The uniqueness of RC route was that it produces highly active catalysts in a single step of calcination route without any secondary activation. The kinetics study of CuMn<sub>RC</sub> catalyst for CO oxidation is done in a fixed bed plug flow reactor, and the kinetic data are collected under the conditions of free heat and mass transfer limitations. Intrinsic rate of air oxidation of CO over CuMnO<sub>x</sub> catalyst is determined as a function of temperature and the concentration in the temperature range of 25-45 °C. The rate of CO oxidation is given by:

$$(-r_p) = 5.856 \times 10^5 \exp(-10839/RT) (C_{CO})^{0.84} \text{ gmol/g}_{\text{cat}} \cdot \text{h}$$

and activation energy is found to be 36.98 kJ/g mol.

#### References

- [1] Xie, X., Li, Y., Liu, Z., Haruta, M., Shen, W. (2009). Low-Temperature Oxidation of CO Catalysed by Co<sub>3</sub>O<sub>4</sub> Nanorods. *Nature Letters*, 458: 746-749.
- [2] Taylor, S.H., Rhodes, C. (2005). Ambient Temperature Oxidation of Carbon Monoxide Using a Cu<sub>2</sub>Ag<sub>2</sub>O<sub>3</sub> Catalyst. *Catalysis Letters*, 101: 31-33.
- [3] Tang, Z.R., Jones, C.D., Aldridge, J.K.W., Davies, T.E., Bartley, J.K., Carley, A.F., Taylor, S.H., Allix, M., Dickinson, C., Rosseinsky, M.J., Claridge, J.B., Xu, Z.L., Crudace, M.J., Hutchings, G.J. (2009). New Nanocrystalline Cu/MnO<sub>x</sub> Catalysts Prepared from Supercritical Antisolvent Precipitation. *Chemcatchem Catalysis*, 1: 247-251.
- [4] Kanungo, S.B. (1979). Physicochemical Properties of MnO<sub>2</sub>, CuO and their Relationship with the Catalytic Activity for H<sub>2</sub>O<sub>2</sub> Decomposition and CO Oxidation. *Journal of Catalysis*, 58: 419-435.
- [5] Schwab, G.M., Kanungo, S.B. (1977). Efficient Stable Catalyst for Low Temperature Carbon Monoxide Oxidation. *Journal of Catalysis*, 107: 109-120.
- [6] Veprek, S.D., Cocke, L., Kehl, S., Oswald, H.R. (1986). Mechanism of the Deactivation of Hopcalite Catalysts Studied by XPS, ISS, and other Techniques. *Journal of Catalysis*, 100: 250-263.
- [7] Taylor, S.H., Hutchings, G.J., Mirzaei, A.A. (1999). Copper Zinc Oxide Catalysts for Ambient Temperature Carbon Monoxide Oxidation. *Chemical Communications*, 15: 1373-1374.
- [8] Cai, L., Guo, Y., Lu, A., Branton, P., Li, W. (2012). The Choice of Precipitant and Precursor in the Co-precipitation Synthesis of Copper Manganese Oxide for Maximizing Carbon Monoxide Oxidation. *Journal of Molecular Catalysis A: Chemical*, 360: 35-41.
- [9] Kramer, M., Schmidt, T., Stowe, K., Maier, W.F. (2006). Structural and Catalytic Aspects of Sol-Gel Derived Copper Manganese Oxides as Low-Temperature CO Oxidation Catalyst. *Applied Catalysis A: General*, 302: 257-263.
- [10] Zhang, W., Zhao, Q., Wang, X., Yan, X., Han, S., Zeng, Z. (2016). Highly Active and Stable Au@Cu<sub>x</sub>O Core-Shell Nanoparticles Supported on Alumina for Carbon Monoxide Oxidation at Low Temperature. *RSC Advances*, 79: 75126-75132.
- [11] Li, L., Chai, S., Binder, A., Brown, S., Yang, S., Dai, S. (2015). Synthesis of MCF-Supported AuCo Nanoparticle Catalysts and

- Catalytic Performance for the CO Oxidation Reaction. *RCS Advances*, 121: 100212-100222.
- [12] Dirany, N., Arab, M., Madigou, V., Leroux, C., Gavarrí, J.R. (2016). A Facile One Step Route to Synthesize WO<sub>3</sub> Nanoplatelets for CO Oxidation and Photo Degradation of RhB: Micro Structural, Optical and Electrical Studies, *RSC Advances*, 73: 69615-69626.
- [13] Guo, X., Zhou, R. (2016). A New Insight into the Morphology Effect of Ceria on CuO/CeO<sub>2</sub> Catalysts for CO Selective Oxidation in Hydrogen-Rich Gas. *RSC, Catalysis Science & Technology*, 11: 3862-3871.
- [14] Chen, C.S., Chen, T.C., Chen, C.C., Lai, Y.T., You, J.H., Chou, T.M., Chen, C.H., Lee, J. (2012). Effect of Ti<sup>3+</sup> on TiO<sub>2</sub> Supported Cu Catalysts Used for CO Oxidation. *ACS publications, Langmuir*, 28: 9996-10006.
- [15] Sun, Y., Lv, P., Yang, J., He, L., Nie, J., Liu, X., Li, Y. (2011). Ultrathin Co<sub>3</sub>O<sub>4</sub> Nanowires with High Catalytic Oxidation of CO. *RSC, Chemical Communications*, 40: 11279-11281.
- [16] Njagi, E.C., Chen, C., Genuino, H., Galindo, H., Huang, H., Suib, S.L. (2010). Total Oxidation of CO at Ambient Temperature Using Copper Manganese Oxide Catalysts Prepared by A Redox Method. *Applied Catalysis B: Environmental*, 99: 103-110.
- [17] Jones, C., Taylor, S.H., Burrows, A., Crudace, M.J., Kiely, C.J., Hutchings, G.J. (2008). Cobalt Promoted Copper Manganese Oxide Catalysts for Ambient Temperature Carbon Monoxide Oxidation. *Chemical Communications*, 1707-1709.
- [18] Zhanga, X., Mab. K., Zhanga, L., Yonga, G., Yadib, M., Liu, S. (2011). Effect of Precipitation Method and Ce Doping on the Catalytic Activity of Copper Manganese Oxide Catalyst for CO Oxidation. *Chinese Journal of Chemical Physics*, 24: 97-102.
- [19] Solsona, B., Hutchings, G.J., Garcia, T., Taylor, S.H. (2004). Improvement of the Catalytic Performance of CuMnOx Catalysts for CO Oxidation by the Addition of Au. *New Journal of Chemistry*, 6: 708-711.
- [20] Dey, S., Dhal, G.C., Prasad, R., Mohan, D. (2016). The Effect of Doping on the Catalytic Activity of CuMnOx Catalyst for CO Oxidation. *Journal of Environmental Science, Toxicology and Food Technology*, 10(11): 86-94.
- [21] Mishra, A., Prasad, R. (2011). A Review on Preferential Oxidation of Carbon Monoxide In Hydrogen Rich Gases. *Bulletin of Chemical Reaction Engineering & Catalysis*, 6(1): 1-14.
- [22] Rattan, G., Prasad, R., Katyal, R.C. (2012). Effect of Preparation Methods on Al<sub>2</sub>O<sub>3</sub> Supported CuO-CeO<sub>2</sub>-ZrO<sub>2</sub> Catalysts for CO Oxidation. *Bulletin of Chemical Reaction Engineering & Catalysis*, 7(2): 112-123.
- [23] Singh, P., Prasad, R. (2014). Catalytic Abatement of Cold-Start Vehicular CO Emissions. *Catalysis and Environmental Protection, Catalysis in Industry*, 6(2): 122-127.
- [24] Clarke, T.J., Davies, T.E., Kondrat, S.A., Taylor, S.H. (2015). Mechano Chemical Synthesis of Copper Manganese Oxide for the Ambient Temperature Oxidation of Carbon Monoxide. *Applied Catalysis B: Environmental*, 165: 222-231.
- [25] Mirzaei, A.A., Shaterian, R.H., Habibi, M., Hutchings, G.J., Taylor, S.H. (2003). Characterization of Copper-Manganese Oxide Catalysts: Effect of Precipitate Ageing upon the Structure and Morphology of Precursors and Catalysts. *Applied Catalysis A: General*, 253: 499-508.
- [26] Cole, K.J., Carley, A.F., Crudace, M.J., Clarke, M., Taylor, S.H., Hutchings, G.J. (2010). Copper Manganese Oxide Catalysts Modified by Gold Deposition: The Influence on Activity for Ambient Temperature Carbon Monoxide Oxidation. *Catalysis Letters*, 138:143-147.
- [27] Granger, P., Lecomte, J.J., Leclercq, L., Leclercq, G. (2001). An Attempt at Modeling the Activity of Pt-Rh/Al<sub>2</sub>O<sub>3</sub> Three-Way Catalysts in the CO+NO Reaction. *Applied Catalysis A: General*, 208(2): 369-379.
- [28] Hasegawa, Y., Maki, R., Sano, M., Miyake, T. (2009). Preferential Oxidation of CO on Copper-Containing Manganese Oxides. *Applied Catalysis A: General*, 371: 67-72.
- [29] Jones, C., Cole, K.J., Taylor S.H., Crudace M.J., Hutchings, G.J. (2009). Copper Manganese Oxide Catalysts for Ambient Temperature Carbon Monoxide Oxidation: Effect of Calcination on Activity. *Journal of Molecular Catalysis A: Chemical*, 305: 121-124.
- [30] Tanaka, Y., Utaka, T., Kikuchi, R., Takeguchi, T., Sasaki, K., Eguchi, K. (2003). Water Gas Shift Reaction for the Reformed Fuels over Cu/MnO Catalysts Prepared via Spinel-Type Oxide. *Journal of Catalysis*, 215: 271-278.